# Computation of Viscous Flows in Turbomachinery Cascades with a Space-Marching Method

M. Pouagare,* B. Lakshminarayana,† and T. R. Govindan‡
*The Pennsylvania State University, University Park, Pennsylvania*

**A space-marching method was used to predict the viscous flowfield in turbomachinery cascades. Departure solutions were suppressed by modifying the streamwise pressure gradient term in the momentum equations. For staggered cascades a nonperiodic grid system was employed, and appropriate approximations were used in place of the periodicity boundary conditions upstream and downstream of the cascade. The laminar flow through a flat-plate cascade at 45-deg stagger and through a symmetric cascade at zero incidence and stagger was tested first. The method was then used to predict the turbulent flow through compressor cascades composed of NACA 65-series blades. The predicted drag coefficient, turning angle, boundary-layer momentum thicknesses, and velocity profiles were compared with the experimental data; the agreement was good in most cases. The solution of the cases presented was obtained in less than 1 min of CPU time on an IBM 3081 computer.**

## Nomenclature

$a$ = angle of attack
$b_1, b_2$ = parameters determining the numerical scheme employed
$C$ = chordlength
$C_D$ = drag coefficient, Eq. (26)
$C_p$ = pressure coefficient, $=(p-p_1)/\frac{1}{2}\rho Q_1^2$
$D$ = diffusion term; drag force
$E, E_s, E_p, F, T, P$ = vectors in the governing equations
$e_i, e$ = specific internal energy and total fluxing energy
$J$ = Jacobian of the grid transformation
$k$ = coefficient of thermal conductivity
$\ell$ = turbulence length scale in a boundary layer
$L$ = semiwake width
$M$ = Mach number
$n$ = streamwise station
$p$ = static pressure
$p_s$ = assumed initial static pressure
$P_r$ = Prandtl number
$Q$ = streamwise velocity
$Q_s$ = velocity defect at the center of the wake
$q$ = dependent vector in the governing equations
$r$ = distance normal to the wall
$Re$ = Reynolds number, $=Q_1 C/\nu$
$S$ = vector containt artificial damping terms, Eq. (12)
$s$ = blade spacing
$u, v$ = velocity in the $x$ and $y$ directions, respectively
$U$ = contravariant velocity component along the $\xi$ coordinate, $=\xi_x u+\xi_y v$
$u^*$ = friction velocity
$V$ = contravariant velocity component along the $\eta$ coordinate, $=\eta_x u+\eta_y v$
$x, y$ = Cartesian coordinates; $x$ is the axial direction, and $y$ the transverse direction
$z$ = distance from the leading edge measured along the chordline
$\alpha$ = angle of the grid lines with the $x$ coordinate
$\beta$ = flow angle (see Fig. 1)
$\gamma$ = ratio of specific heats
$\Delta m$ = change in the global mass flow
$\Delta P_0$ = total pressure difference across the cascade
$\delta$ = boundary-layer thickness
$\zeta$ = loss coefficient, Eq. (25)
$\theta$ = momentum thickness normalized by $C$
$\lambda$ = stagger angle (Fig. 1)
$\mu_T$ = eddy viscosity
$\nu$ = kinematic viscosity
$\xi, \eta$ = body-fitted coordinate system
$\xi_x, \eta_x, \xi_y, \eta_y$ = metric coefficients in the grid transformation
$\rho$ = density
$\phi$ = angle between $\xi$ and $\eta$ grid lines
$\psi_1, \psi_2$ = viscous dissipation terms in the energy equation
$\omega$ = fraction of streamwise pressure gradient kept implicitly

*Superscripts*

$n$ = streamwise station index
$\hat{()}$ = vectors in the governing equations in the computational domain

*Subscripts*

$c$ = correction values
$p$ = quantity at the first grid point away from the wall
ss,ps = suction side and pressure side, respectively
TE = trailing-edge values
$xy, \xi\eta$ = quantities in the $(x,y)$ and $(\xi,\eta)$ coordinates, respectively
1,2 = upstream and downstream of the cascade, respectively
$\infty$ = quantity at the edge of the boundary layer

Received July 29, 1985; revision received Dec. 16, 1985. 

*Department of Aerospace Engineering; presently, Assistant Professor of Mechanical Engineering, Duke University, NC.

†Department of Aerospace Engineering; presently, Research Scientist, Scientific Research Associates Inc., Glastonbury, CT.

‡Distinguished Alumni Professor of Aerospace Engineering, Director of Computational Fluid Dynamics Studies, Department of Aerospace Engineering. Fellow AIAA.

## Introduction

KNOWLEDGE of the flowfield through a cascade of blades is essential for turbomachinery design. In the early stages of jet engine development, turbomachinery designers depended largely on experimental data to derive the performance characteristics of cascades. However, experimental data are difficult and time-consuming to obtain. This difficulty has motivated research to predict the performance of cascades with numerical methods.

In the past two decades, considerable progress has been made in the prediction of the inviscid flow through cascades.[1] However, little progress has been made in predicting the viscous flow. The existing time-marching algorithms that can predict the viscous flow are expensive.[2,3]

The boundary-layer approximation,[4] though economical, is difficult to implement in internal flows because of the displacement effects of the boundary layer on the inviscid flow.

This paper presents an economical algorithm for the prediction of the viscous flowfield through turbomachinery cascades. The algorithm is based on the parabolized Navier-Stokes equations, which are solved with the space-marching technique developed by Govindan.[5]

The present algorithm requires a knowledge of the streamwise pressure gradient, as the boundary-layer approximation does; but, unlike the boundary-layer approximation, the present algorithm solves the equations in the entire flowfield.

Space- (or parabolic-) marching techniques have been widely used for the prediction of the flow through curved channels. However, the prediction of the flowfield in cascades presents difficulties that are not found in the prediction of the flowfield in curved channels. The most distinct differences are the following:

1) Periodicity of the flow must be enforced upstream and downstream of a cascade.

2) The stagnation point at the leading edge of a cascade causes strong streamwise pressure gradients.

3) The rapid change in the boundary shape near the leading edge of a cascade introduces additional problems.

4) It is difficult to keep the grid orthogonal everywhere in a cascade.

The abovementioned problems must be overcome for the accurate prediction of the viscous flowfield in cascades.

The method was first tested in two hypothetical cases. The first case was a flat-plate cascade with zero thickness, a zero angle of attack, a space-to-chord ratio of unity, and a stagger angle of 45 deg. This test case was used to study the problems associated with the stagger angle (nonorthogonal grid) and the periodicity boundary condition. The second test case was an NACA 65-010 cascade with zero inlet and exit flow angles, zero stagger, and a space-to-chord ratio of unity. This test case was used to study the problems associated with the leading-edge stagnation point and the rapid changes in the boundary shape near the leading edge. Finally, the method was tested for cascades used in practice. The predicted exit flow angle, d coefficient, boundary-layer profiles, and boundary-la momentum thicknesses were compared with the available perimental data; agreement between them was found to good.

A modified version of the space-marching code developed by Govindan[5] was used in the computation.

## The Governing Equations and the Space-Marching Method

Details of the space-marching method are given by Govindan,[5] therefore, only a brief description will be given in this section. Some modifications made to this code are also described in this section.

The nondimensionalized, steady, two-dimensional, compressible Navier-Stokes equations can be written in conservation-law form as follows:

$$\frac{\partial E(q)}{\partial x}+\frac{\partial F(q)}{\partial y}=\frac{1}{Re}\left[\frac{\partial T(q)}{\partial x}+\frac{\partial P(q)}{\partial y}\right] \tag{1}$$

where

$$q=[\rho,\rho u,\rho v,\rho e_i]^T \tag{2}$$

The vectors $E$, $F$, $T$, and $P$ are given in the Appendix. The fluxing internal energy ($\rho e_i$) was used instead of the more commonly used total energy $e$. The use of $\rho e_i$ instead of $e$ as an independent variable was found to improve the solution for low Mach number flows.

To facilitate the application of the boundary conditions, a body-fitted coordinate system was used. The body-fitted grid in the physical domain was transformed into a rectangular grid in the computational domain by the transformation

$$\xi=\xi(x,y), \qquad \eta=\eta(x,y) \tag{3}$$

where $\xi$ is the coordinate in the near-streamwise direction, and $\eta$ the coordinate in the transverse direction.

Equation (1) was transformed into the body-fitted coordinate system $(\xi,\eta)$. The resulting equation can be kept in the same form as Eq. (1)

$$\frac{\partial \hat{E}(q)}{\partial \xi}+\frac{\partial \hat{F}(q)}{\partial \eta}=\frac{1}{Re}\left[\frac{\partial \hat{T}(q)}{\partial \xi}+\frac{\partial \hat{P}(q)}{\partial \eta}\right] \tag{4}$$

where

$$\hat{E}=\frac{\xi_x}{J}E+\frac{\xi_y}{J}F, \quad \hat{F}=\frac{\eta_x E}{J}+\frac{\eta_y F}{J}$$

$$\hat{T}=\frac{\xi_x}{J}T+\frac{\xi_y}{J}P, \quad \hat{P}=\frac{\eta_x}{J}T+\frac{\eta_y}{J}P$$

and $J$ is the Jacobian of the coordinate transformation given by

$$J=\xi_x\eta_y-\xi_y\eta_x \tag{5}$$

For flows with a dominant flow direction, the Navier-Stokes equations can be parabolized by neglecting the streamwise diffusion terms. Also, the streamwise pressure gradient in the momentum equation must be evaluated in a special way in order to avoid departure solutions.[6,7] Therefore, the Navier-Stokes equations were parabolized by dropping the term $\partial T/\partial\xi$ in Eq. (4), and by writing the term $\partial E/\partial\xi$ as

$$\frac{\partial \hat{E}}{\partial \xi}=\frac{\partial \hat{E}_s(q)}{\partial \xi}+\hat{E}_p(p_s) \tag{6}$$

$$\hat{E}_s(q)=\frac{1}{J}[\rho u,\rho uU+\xi_x(2\omega-1)p,$$

$$\rho vU+\xi_y(2\omega-1)p,\ (e+p)u]^T \tag{7}$$

$$\hat{E}_p(p_s)=\left(\frac{1-\omega}{J}\right)\frac{p_s^{n+1}-p_s^n}{\xi}[0,\xi_x,\xi_y,0]^T \tag{8}$$

where $\omega$ is given by[7]

$$\omega=\gamma M^2/[1+(\gamma-1)M^2] \tag{9}$$

and is required to prevent branching.

The parabolized Navier-Stokes equations are written as

$$\frac{\partial \hat{E}_s(q)}{\partial \xi}+\hat{E}_p(p_s)+\frac{\partial \hat{F}(q)}{\partial \eta}=\frac{1}{Re}\frac{\partial \hat{P}(q)}{\partial \eta} \tag{10}$$

Equation (10) is a well-posed initial value problem that governs the evolution of the flux vector $\hat{E}_s$. Starting from an initial $\eta$ line, the solution is marched downstream in the $\xi$ direction, which is the "time-like" coordinate. $\hat{E}_p(p_s)$ is estimated from the pressure at $(n+1)$ calculated from an inviscid code and the pressure at $(n-1)$ calculated by the present method.

**The Numerical Technique**

Following Beam and Warming,[8] Eq. (10) is finite-differenced as follows:

$$\left[\left(\frac{\partial \hat{E}_s}{\partial q}\right)^n - \frac{b_1\Delta\xi}{1+b_2}\left[\frac{\partial}{\partial\eta}\left(\frac{\partial B}{\partial q}\right)^n\right]\right]\Delta q^n = \frac{b_2}{1+b_2}\left[\frac{\partial \hat{E}_s}{\partial q}\right]^{n-1}\Delta q^{n-1} + \frac{b_1\Delta\xi}{1+b_2}(N^n - N^{n-1}) + \frac{\Delta\xi}{1+b_2}\left[\frac{\partial B}{\partial\eta} + N\right]^n \tag{11}$$

where

$$B = \frac{\hat{P}}{Re} - \hat{F}, \quad N = -\hat{E}_p, \quad q^n = q^n - q^{n-1}$$

The parameters $b_1$ and $b_2$ determine the scheme employed. The present results were obtained with $b_1 = 1$, $b_2 = \frac{1}{2}$ corresponding to a three-point backward implicit scheme with a truncation error $\mathcal{O}(\Delta\xi^3)$.

In order to prevent the uncoupling of the odd and even points, a second-order artificial dissipation term was added to Eq. (11) on both the explicit and implicit sides. This term has the form

$$S = \frac{1}{J}\left[\sigma_1\frac{\partial^2\rho}{\partial\eta^2}, \sigma_2\frac{\partial^2(\rho u)}{\partial\eta^2}, \sigma_3\frac{\partial^2(\rho v)}{\partial\eta^2}, \sigma_4\frac{\partial^2(\rho e_i)}{\partial\eta^2}\right]^T \tag{12}$$

where $\sigma_1$, $\sigma_2$, $\sigma_3$, and $\sigma_4$ are the damping coefficients. The coefficients $\sigma_2$ and $\sigma_3$ were carefully chosen so that the damping terms $S_2$ and $S_3$ were much smaller than the second-order viscous terms in regions where viscous terms are significant.

**Global Mass Flow and Pressure and Velocity Corrections**

In calculating a flowfield with a space-marching method, an initial velocity profile must be specified at the initial station. This specification determines the global mass flow in an internal flow computation. Furthermore, the streamwise pressure gradient is approximated from the assumed pressure field. However, in an internal flow computation, the specification of the global mass flow and the streamwise pressure gradient is mutually exclusive. In an internal flow computation where the global mass flow is specified and the streamwise pressure gradient approximated, requirements of uniqueness of the solution and the linearization errors in the numerical scheme lead to a slow loss of the global mass flow constraint.[5] Maintenance of this constraint is important in internal flow computations, and, therefore, the streamwise pressure gradient must be adjusted to prevent loss of the constraint. In the present algorithm, this is done as follows:

1) After the solution is found at a particular streamwise station $n$, the change in the total mass flow is calculated, and the corrections to the streamwise pressure gradients and the velocity are derived from the following approximate formulas:

$$P_{sc} = -m\Big/\int_\eta \frac{\xi_x^2 + \xi_y^2}{JU}d\eta,$$

$$u_c = -\frac{\xi_x}{\rho U}P_{sc}, \quad v_c = -\frac{\xi_y}{\rho U}P_{sc} \tag{13}$$

2) The pressure correction is used to correct the streamwise pressure gradient to be used in the solution of the next streamwise station $n+1$. The velocity corrections are used to correct the velocity at the current streamwise station $n$.

The corrections to the presure gradient and velocity were found to be small at each streamwise station.

## The Grid System

For the numerical solution of the flowfield in cascades, the most convenient body-fitted grid is the H-type grid (see Fig. 1). The periodicity boundary condition upstream and downstream of the cascade requires that the two extremes of the $\eta$ lines be periodic points. This implies that the $\xi$ and $\eta$ lines intersect approximately at an angle equal to the stagger angle. The nonorthogonality of the $\xi$ and $\eta$ lines should not present any problems since the transformation expressed by Eq. (3) is general, and no assumption of orthogonality was made. However, only a simplified form of the Navier-Stokes equations is being solved, and the approximations made are not necessarily independent of the coordinate system. In order to see this dependence, consider the flow over a flat plate with the $x$ and $\xi$ coordinates along the flat plate, the $y$ coordinate normal to $x$, and $\eta$ forming an angle $\phi$ with $\xi$ (see Fig. 2). For this geometry, the coordinate transformation is given by

$$\xi = x - \cot\phi y, \qquad \eta = y \tag{14}$$

Consider the diffusion term in the $x$-momentum equation for incompressible flow

$$D_{xy} = \frac{1}{Re}\left[\frac{\partial^2 u}{\partial x^2} + \frac{\partial^2 u}{\partial y^2}\right] \tag{15}$$

The $xy$ index indicates that the diffusion $D$ is considered in the $x,y$ coordinate system.

Transforming Eq. (15) to $(\xi,\eta)$ coordinates, and assuming that all metrics are constant throughout the domain of in-

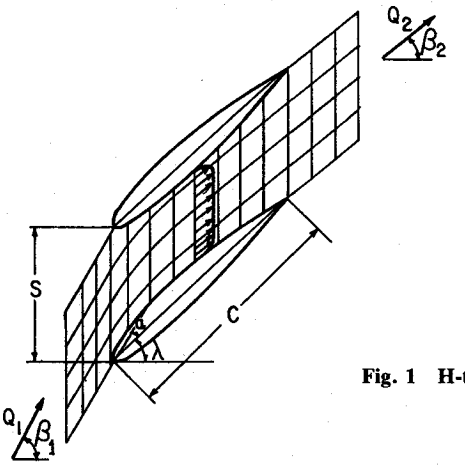


**Fig. 1 H-type periodic grid.**

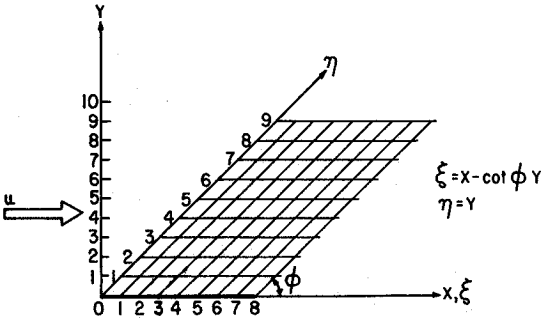


**Fig. 2 Nonorthogonal $\xi$-$\eta$ coordinate system for the flow over a flat plate.**

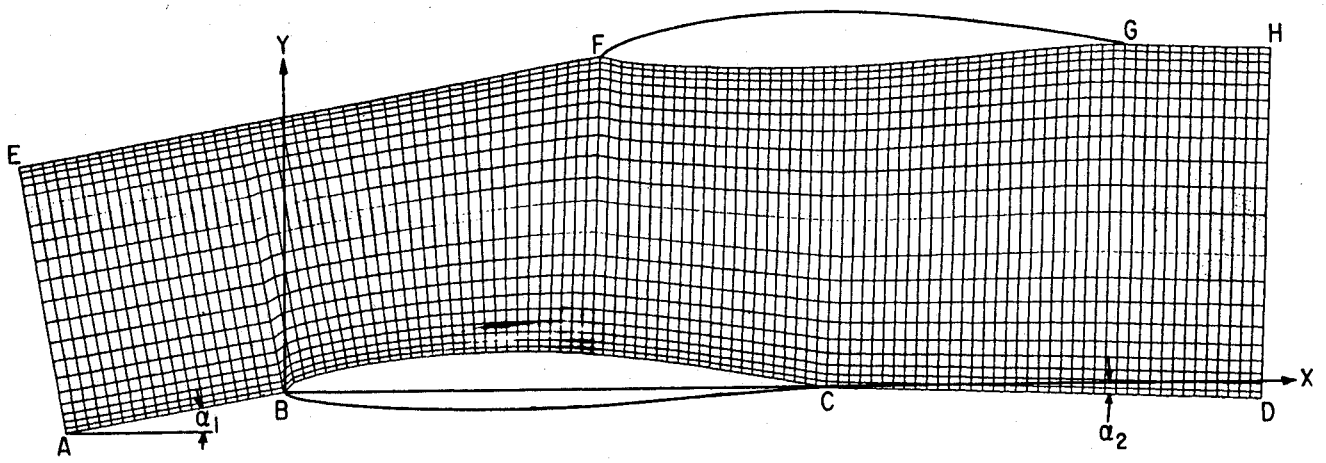


Fig. 3 H-type nonperiodic grid.

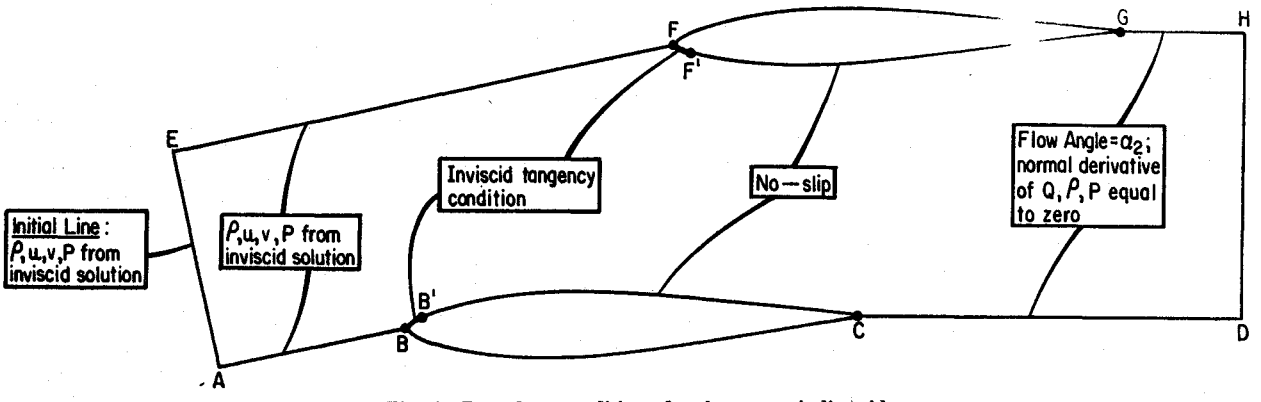


Fig. 4 Boundary conditions for the nonperiodic grid.

terest, the following expression is obtained:

$$D_{\xi\eta}=\frac{1}{Re}\left[(\xi_x^2+\xi_y^2)\frac{\partial^2 u}{\partial\xi^2}+(\eta_x^2+\eta_y^2)\frac{\partial^2 u}{\partial\eta^2}+2(\xi_x\eta_x+\eta_y\xi_y)\frac{\partial}{\partial\xi}\left[\frac{\partial u}{\partial\eta}\right]\right] \tag{16}$$

After neglecting the streamwise diffusion terms, $D_{\xi\eta}$ becomes

$$D^*_{\xi\eta}=\frac{1}{Re}(\eta_x^2+\eta_y^2)\frac{\partial^2 u}{\partial\eta^2} \tag{17}$$

When $D_{\xi\eta}$ is transformed back to $(x,y)$ coordinates, $D_{xy}$ will be obtained as given by Eq. (15). However, transforming $D^*_{\xi\eta}$ back to $(x,y)$ coordinates, the following expression is obtained:

$$D^*_{xy}=\frac{1}{ReJ^2}\left[(\eta_x^2\xi_y^2+\eta_y^2\xi_y^2)\frac{\partial^2 u}{\partial x^2}+(\eta_y^2\xi_x^2+\xi_x^2\eta_x^2)\frac{\partial^2 u}{\partial y^2}-2(\eta_x^2+\eta_y^2)\xi_x\xi_y\frac{\partial^2 u}{\partial x\partial y}\right] \tag{18}$$

For the particular example of the flat plate (Fig. 2), Eq. (18) becomes

$$D^*_{xy}=\frac{1}{Re}\left[(\cot\phi)^2\frac{\partial^2 u}{\partial x^2}+\frac{\partial^2 u}{\partial y^2}+2\cot\phi\frac{\partial^2 u}{\partial x\partial y}\right] \tag{19}$$

Equation (19) indicates that, depending on the angle $\phi$, part of the streamwise diffusion is retained in $D^*_{xy}$ and $D^*_{\xi\eta}$. Only when $\phi=90$ deg (i.e., when $\xi,\eta$ is an orthogonal coordinate system), the streamwise diffusion terms in $D^*_{xy}$ and $D^*_{\xi\eta}$ are zero.

A similar analysis of the streamwise pressure gradient term[9] showed that the assumption made concerning this term is strictly valid only for an orthogonal $(\xi,\eta)$ grid system. Therefore, the basic assumptions used to parabolize the Navier-Stokes equations do not hold for a nonorthogonal grid system.

Numerical experiments of the laminar flow on a flat plate (Fig. 2) indicated that the solution depended on the angle $\phi$, and that the correct solution (Blasius solution) was obtained only with $\phi=90$ deg.

In a recent publication, Degani and Steger[10] compared the results of the thin Navier-Stokes equations with those of the full Navier-Stokes equations for the flow over a ramp. They indicated that the agreement between the two sets of results remained good only when the $\xi$ and $\eta$ lines intersected at an angle greater than 70 deg. Further discussion on the use of an orthogonal grid and parabolizing errors which may be introduced in a transformation can be found in Refs. 11 and 12, respectively.

As has been shown, it is important to keep the $\xi$ and $\eta$ lines as close to being orthogonal as possible. For the flow through staggered cascades, this requires the use of a nonperiodic grid. In the present investigation, a nonperiodic grid is generated algebraically as follows (see Fig. 3):

1) The $x$ coordinate is aligned with the chordline.

2) The lower boundary is formed by a straight line AB forming an angle $\alpha_1$ with the $x$ axis, the suction side of the airfoil BC, and a second straight line CD forming an angle $\alpha_2$ with the $x$ axis.

3) The upper boundary is formed by a straight line EF parallel to AB, the pressure side of the airfoil FG, and a second straight line GH parallel to CD.

4) The $\eta$ lines are straight lines drawn normal to the lower surface along AB and CD. Along BC, the $\eta$ lines are drawn normal to the suction surface wherever the slope of the surface $\tan\alpha$ satisfied the condition

$$\tan\alpha_2 \leq \tan\alpha \leq \tan\alpha_1$$

If $\tan\alpha > \tan\alpha_1$, the $\eta$ lines are drawn parallel to the normal on AB, and if $\tan\alpha < \tan\alpha_2$, the $\eta$ lines are drawn parallel to the normal on CD.

5) Angle $\alpha_1$ need not be related to the flow direction; $\alpha_1$ is that angle which permits most $\eta$ lines to be normal to the $\xi$ lines. Angle $\alpha_2$ is more difficult to find; it has to follow the direction of the exit flow. A detailed discussion on $\alpha_2$ follows in the next section.

6) The spacing in the $\eta$ direction is found. Grid points are clustered near the two extremes of the $\eta$ lines through an exponential function. When the spacing in the $\eta$ direction is found, the $\xi$ lines are drawn. The grid system generated by the preceding method is nearly orthogonal in the whole domain except in the immediate vicinity of the leading edge.

## Initial and Boundary Conditions

### Initial Conditions

The required inviscid pressure distribution for calculating $\hat{E}_p(p_s)$ is obtained from a modified version of the Douglas-Neumann cascade program. The space-marching solution starts from the initial line AE as shown in Fig. 4. All of the required quantities $(\rho,u,v,p)$ are obtained from the inviscid solution. The present method does not capture the elliptic effects; these are all included in the initial pressure distribution prescribed. Therefore, the calculation need not start from far upstream of the leading edge. The solution can start from anywhere upstream of the leading edge or even just at the leading edge.

### Boundary Conditions Upstream of the Leading Edge

The most appropriate boundary condition upstream of the leading edge is the periodicity condition. However, the grid system employed does not allow for the application of the precise periodic boundary condition. In the region of boundary lines AB and EF, the viscous effects are negligible, and, therefore, the known inviscid values of velocity, pressure, and density are used on these lines as boundary conditions. The periodicity condition is thus satisfied since the inviscid solution is periodic.

### Boundary Conditions on the Blade Surfaces

In a viscous calculation, no-slip boundary conditions must be used on solid surfaces. However, in the present investigation the tangency inviscid condition was used near the leading edge (BB' and FF' in Fig. 4). The flow in the interior points does not follow the rapid change of the boundary shape if the no-slip condition is applied in this region. The extent of BB' and FF' is approximately 5% of the chord. Downstream of B' and F', the no-slip boundary condition is used for laminar flow, for turbulent flow a slip condition is used. The latter is discussed in the next section. The use of an inviscid boundary condition during the initial 5% of the chord does not affect the final solution since the boundary-layer thickness in this region is smaller than the distance between the wall and the first grid point away from the wall. The authors feel that the inviscid tangency condition near the leading edge can be avoided if a large number of grid points is used in this region and the thin boundary layer is properly resolved.

### Boundary Conditions Downstream of the Trailing Edge

The most appropriate boundary condition downstream of the trailing edge is the periodicity condition. However, as in the case of the upstream boundary condition, the grid system employed does not allow for the application of the precise periodic boundary condition. The problem downstream is

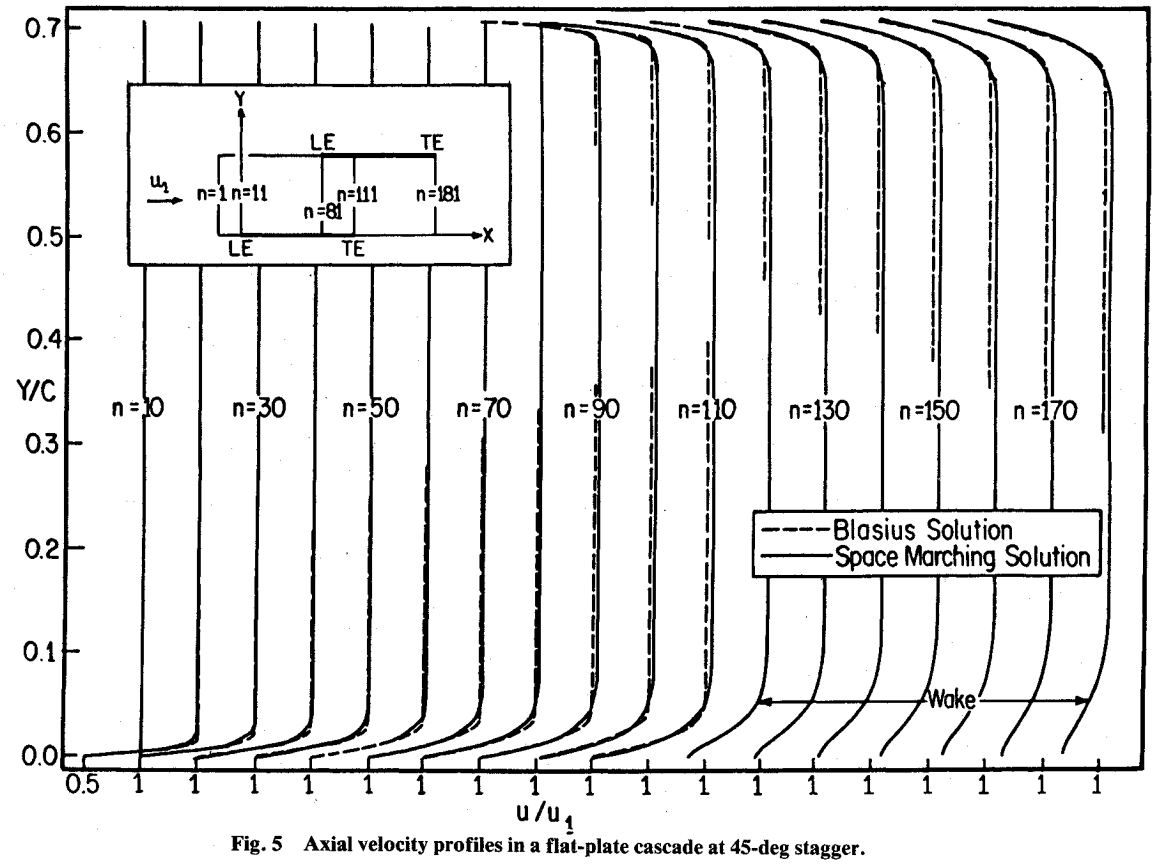


Fig. 5 Axial velocity profiles in a flat-plate cascade at 45-deg stagger.

more severe than that upstream of the cascade, since the inviscid solution cannot be used because of the presence of the wake in this region. Instead, lines CD and GH are chosen to be along the exit flow direction as estimated from experimental data or correlations. The normal derivative of the streamwise velocity, density, and pressure is zero along DC and GH,

$$\frac{\partial \rho}{\partial \eta}=\frac{\partial p}{\partial \eta}=\frac{\partial Q}{\partial \eta}=0$$

This boundary condition is an approximation to the true boundary condition that should be used in the wake region; it is not valid when the wake center follows a highly curved path.

## Turbulence Closure Model

In order to model the effects of turbulence, Prandtl's mixing-length hypothesis is used for the boundary layer and wake.

For the boundary layer, the eddy viscosity is calculated from the formula

$$\mu_T=\rho \ell^2\left[\frac{\partial Q}{\partial r}\right]Re$$

with

$$\ell=\kappa r \quad \text{for } r/\delta \le 0.219$$

$$=0.09\delta \quad \text{for } r/\delta > 0.219 \tag{20}$$

where $Q$ is the streamwise velocity, $r$ the normal distance from the wall, and $\kappa$ the von Kármán constant ($\kappa=0.41$). For the wake, $\mu_T$ is calculated from the formula[13]

$$\mu_T=\rho c L Q_S Re, \quad \text{with} \quad c=0.094 \tag{21}$$

where $Q_S$ is the velocity defect at the center of the wake, and $L$ the wake semiwidth; $L$ is defined as the distance between the center of the wake and the point where the velocity defect is equal to $Q_S/2$.

The calculation of the eddy viscosity is lagged one streamwise step. The mean flow equations are first solved at station $n$ using the eddy viscosity derived at the previous station $n-1$. The derived mean flow quantities at station $n$ are then used to calculate the eddy viscosity to be used at station $n+1$.

In order to avoid the use of a large number of grid points near the wall, a wall function is used to estimate a slip velocity. Following Kreskosky et al.,[14] the wall slip velocity is derived by assuming that the velocity profile is logarithmic at the first grid point away from the wall. Therefore, the velocity gradient at the first grid point away from the wall is given by

$$\frac{\partial Q_p}{\partial r}=\frac{u_*}{\kappa r_p} \tag{22}$$

The index $p$ indicates the quantities at the first grid point away from the wall. Using a backward finite difference, the wall slip velocity is estimated from Eq. (22) as

$$Q_{\text{slip}}=Q_p-\frac{u_*}{\kappa} \tag{23}$$

The friction velocity $u_*$ is found from the law of the wall written at the first grid point away from the wall:

$$\frac{Q_p}{u_*}=\frac{1}{\kappa}\ell n\left(9\frac{u_* r_p}{\nu}Re\right) \tag{24}$$

The first grid point away from the wall is chosen such that it is outside the laminar sublayer and in the law-of-the-wall region.

## Results and Discussion

### Flat-Plate Cascade at 45-deg Stagger

This method was first tested for the laminar flow ($Re=10^4$) through a flat-plate cascade with zero thickness, a zero angle of attack, a space-to-chord ratio of unity, and a stagger angle of 45 deg. For such a cascade, the inviscid flow solution gives uniform pressure everywhere, and, thus, if the boundary-layer

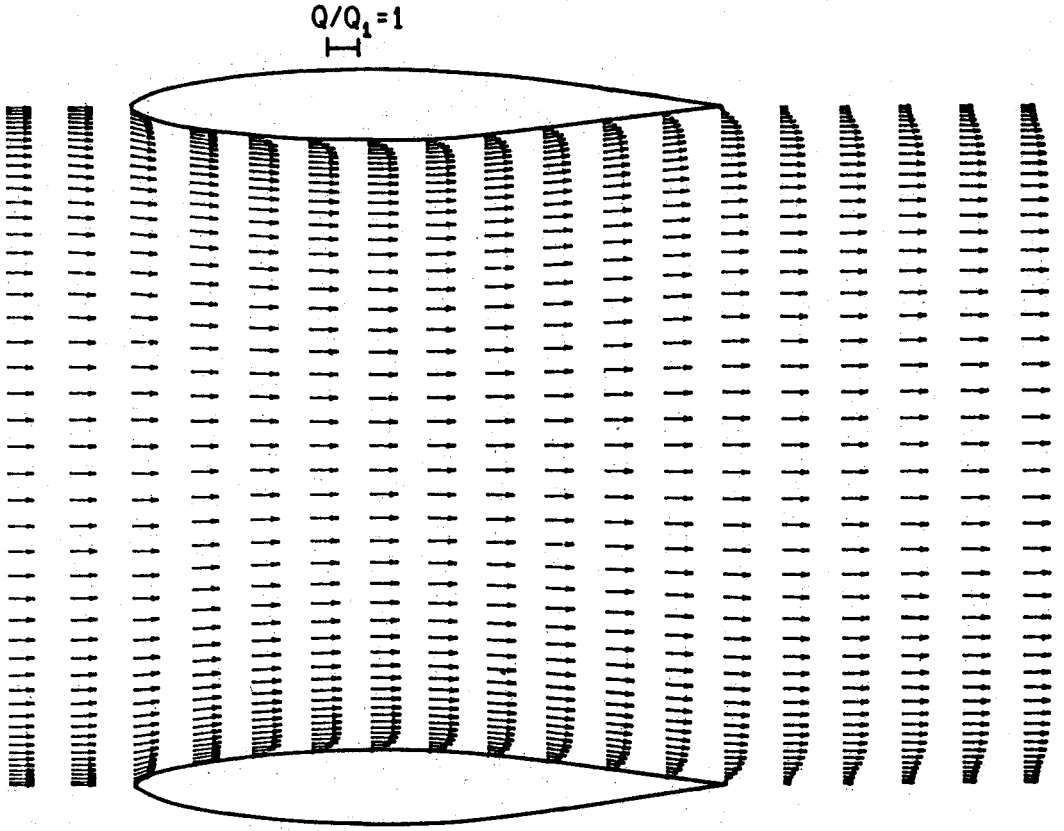


**Fig. 6 Velocity vectors in a symmetric cascade.**

approximation is employed, the viscous solution is given by the Blasius solution.

When the periodic grid ($\xi$ and $\eta$ lines intersecting at 45 deg) was used in the solution, the growth of the boundary layer on the lower surface was very different from the growth on the upper surface, and both were very different from the Blasius solution. This resulted from the nonorthogonality of the grid. The growth of the boundary layer was very different on the two surfaces because the term $2\cot\phi(\partial^2 u/\partial x\partial y)$ in Eq. (19) had a different sign on each surface ($\phi = 45$ deg on the lower surface, and 135 deg on the upper surface).

The axial velocity profiles obtained with the nonperiodic grid are compared with the Blasius solution in Fig. 5. One hundred-streamwise steps per chordlength and 49 grid points in the $\eta$ direction were used in the computation. Figure 5 shows that the present solution captures the core flow acceleration resulting from the development of the boundary layers on the two surfaces. Considering that there are only 2-12 grid points in the boundary layer, the results of the space-marching method are reasonably close to the Blasius solution if the core flow acceleration is neglected.

### Symmetric Cascade

The method was tested next for the laminar flow ($Re = 10^4$) through a cascade composed of NACA 65-010 airfoils, with zero inlet and exit flow angles, zero stagger, and a space-to-chord ratio of unity. One-hundred steps per chordlength and 49 grid points in the $\eta$ direction were used in the computation. Figure 6 shows the calculated velocity vectors. The space-marching method responds well to the strong streamwise pressure gradients present near the leading edge, and captures the acceleration of the core flow resulting from the development of the boundary layers on the two surfaces. The flow follows the boundary shape everywhere, including the leading-edge region.

### Herrig et al.'s Cascade[15]

The turbulent flow through a cascade composed of NACA 65-010 airfoils, experimentally tested by Herrig et al.,[15] was computed with the present method at two different angles of attack ($a = 4$ and 8 deg). The parameters of the two cases are given in Table 1. Two-hundred steps per chordlength and 49 grid points in the $\eta$ direction were used in the calculation. The predicted momentum thicknesses on both surfaces at the two angles of attack are shown in Fig. 7. Using the predicted momentum thicknesses at the trailing edge, the loss coefficient $\zeta$ was calculated from Speidel's[16] formula

$$\zeta = \frac{\Delta P_0}{\frac{1}{2}\rho Q_1^2} = \frac{2(\theta_{ss} + \theta_{ps})_{TE}}{\cos^3\beta_2 \cos^{-2}\beta_1}\left(\frac{C}{S}\right) \tag{25}$$

Then, the drag coefficient was calculated from the relationship

$$C_D = \frac{D}{\frac{1}{2}\rho Q_1^2 C} = \zeta\left(\frac{s}{c}\right)\cos\beta_m \tag{26}$$

where $\beta_m = (\tan\beta_1 + \tan\beta_2)/2$.

The predicted $C_D$ as well as the predicted turning angle are compared with the measured values in Table 2. The agreement between the predicted and measured values is good. The differences in the values of $C_D$ cannot be considered high since $C_D$ is a small quantity and difficult to measure.

**Table 1 Cascade parameters**

| | | |
|---|---|---|
| Angle of attack, deg | 4 | 8 |
| Inlet flow angle, deg | 30 | 30 |
| Space-to-chord angle | 1 | 1 |
| Stagger angle, deg | 26 | 22 |

### Peterson's Cascade[17]

Peterson measured the boundary layer developing on a cascade composed of NACA 65-410 airfoils. The parameters of the cascade were as follows: $a = 10$ deg, $\lambda = 45$ deg, and $s/c = 0.85$.

Two-hundred steps per chordlength and 49 grid points in the $\eta$ direction were used in the calculation. The solution was started at 5% of the chordlength downstream of the leading edge on the lower surface (see insert in Fig. 8).

The predicted streamwise velocity profiles as well as those obtained from the Douglas-Neumann inviscid code are shown in Fig. 8. This figure shows that the viscous effects alter the inviscid velocity distribution. This is prominent at the trailing-edge region.

The predicted boundary-layer profiles on the suction and pressure sides are compared with those measured in Figs. 9

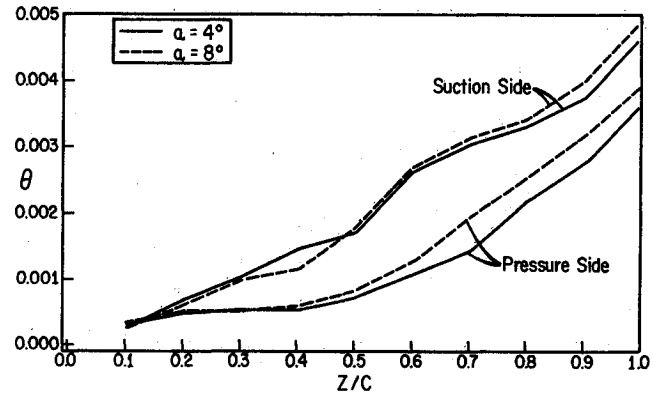


**Fig. 7 Boundary-layer momentum thickness in Herrig et al.'s cascade.[15]**

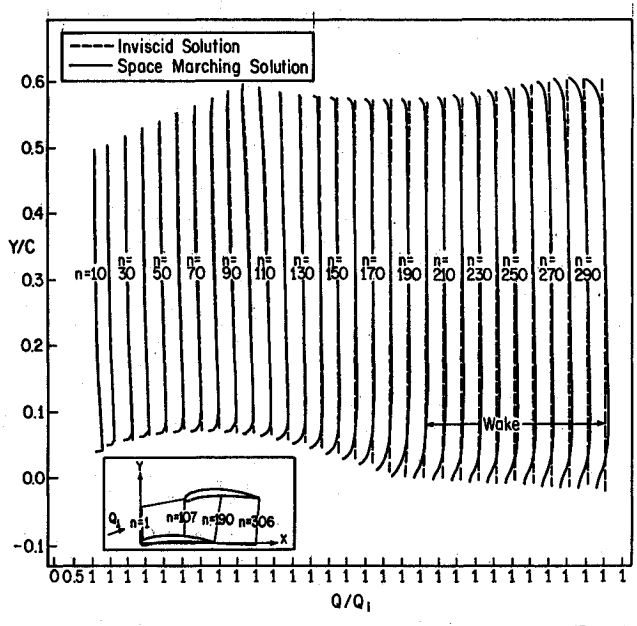


**Fig. 8 Streamwise velocity profiles in Peterson's casade.[17]**

**Table 2 Predicted and measured $C_D$ and $\beta_2 - \beta_1$ for an NACA 65-010 cascade**

| $a$, deg | $C_D$ measured, | $C_D$ predicted, | $\beta_2 - \beta_1$ measured, deg | $\beta_2 - \beta_1$ predicted, deg |
|---|---|---|---|---|
| 4 | 0.0125 | 0.0152 | 3 | 2.5 |
| 8 | 0.0125 | 0.0150 | 7 | 6.6 |

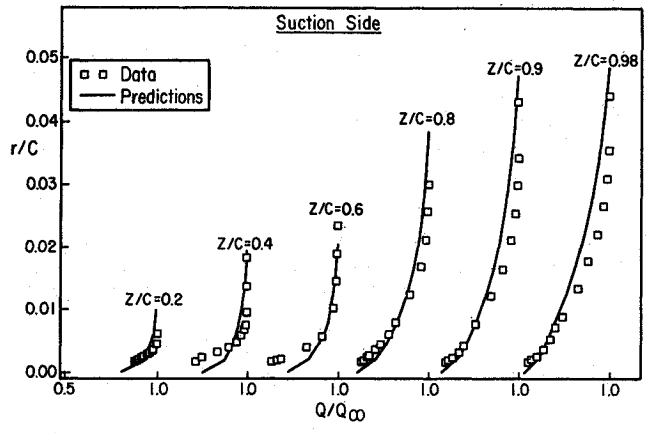


Fig. 9 Boundary-layer profiles on the suction side of Peterson's cascade.[17]

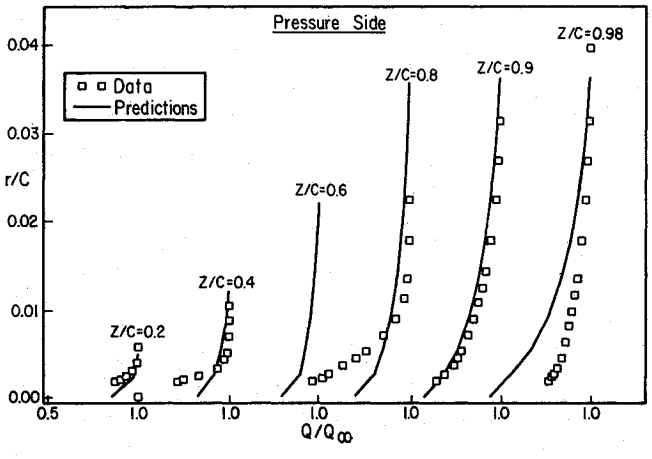


Fig. 10 Boundary-layer velocity profiles on the pressure side of Peterson's cascade.[17]

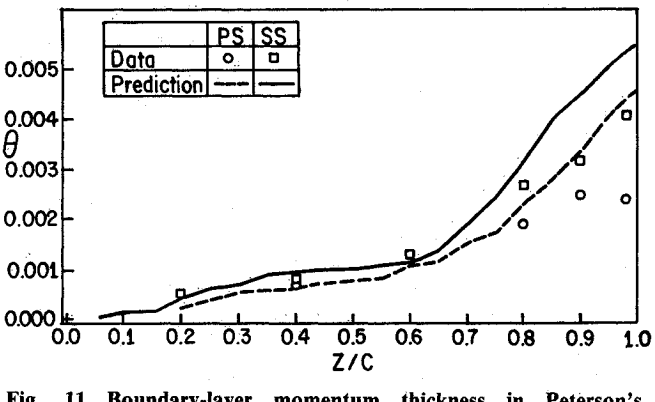


Fig. 11 Boundary-layer momentum thickness in Peterson's cascade.[17]

and 10, respectively. The agreement between the two is good on the suction side. However, on the pressure side, the agreement is good only at $z/C=0.9$. The data at the last three locations on the pressure side ($z/C=0.8$, 0.9, 0.98) does not seem correct since the velocity defect near the wall decreases with increasing $z'/C$.

The predicted and measured momentum thicknesses are compared in Fig. 11. The agreement is good up to 80% of the chord.

One possible reason for the discrepancies between the predicted and measured values is the inaccurate initial inviscid

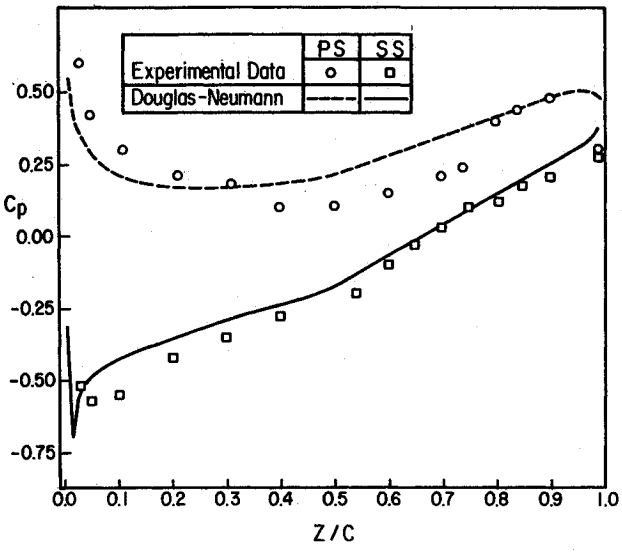


Fig. 12 Blade pressure distribution in Peterson's cascade.[17]

pressure distribution. Figure 12 shows the measured blade pressure distribution as well as that predicted from the Douglas-Neumann program. The pressure gradients are comparable only on the suction side up to 80% of the chord. The results of the space-marching code can be improved through the employment of a global iteration scheme.

## Concluding Remarks

The present investigation has demonstrated that the space-marching method can predict the viscous flow in turbomachinery cascades. The necessity of keeping the grid nearly orthogonal has been demonstrated. A nearly orthogonal, nonperiodic grid system for cascades has been proposed along with the boundary conditions that must be used. Second-order artificial damping terms were used to avoid uncoupling of the odd and even points in the inviscid region of the flowfield.

Rothmayer and Davis[18] showed that the interaction mechanism in a cascade tends to become very localized as the cascade spacing decreases. In addition, the region over which upstream influence is important becomes smaller for decreasing cascade spacing. This confirms the usefulness of the space-marching technique to cascade flows. The technique presented in this paper incorporates the localized interaction and neglects only the interaction that involves upstream influence. It should be easier to correct the marching technique to allow for upstream influence in a cascade, as opposed to external flows.

Presently, this method cannot be used in cascades where the flow is separated and/or when the cascade blade has a blunt leading edge.

One of the major advantages of the method is that it is economical; the solution for Peterson's cascade on a 306 × 49 grid was obtained in about 50 s of CPU time on an IBM 3081. The accuracy of the method is good, but can be improved upon by using a global iteration technique.

## Appendix

The vectors $E$, $F$, $T$, and $P$ in Eq. (1) are given by the following expressions:

$$E=\begin{bmatrix}\rho u\\ \rho u_2+p\\ \rho uv\\ (e+p)u\end{bmatrix},\quad F=\begin{bmatrix}\rho v\\ \rho uv\\ \rho v^2+p\\ (e+p)e\end{bmatrix}$$

$$T = \begin{bmatrix} 0 \\ 2\mu\dfrac{\partial u}{\partial x} - \dfrac{2}{3}\mu\left(\dfrac{\partial u}{\partial x} + \dfrac{\partial v}{\partial y}\right) \\ \mu\left(\dfrac{\partial v}{\partial x} + \dfrac{\partial u}{\partial x}\right) \\ \mu\dfrac{k\gamma}{Pr}\dfrac{\partial e_i}{\partial y} + \psi_1 \end{bmatrix}$$

$$P = \begin{bmatrix} 0 \\ \mu\left(\dfrac{\partial v}{\partial x} + \dfrac{\partial u}{\partial x}\right) \\ 2\mu\dfrac{\partial v}{\partial y} - \dfrac{2}{3}\mu\left(\dfrac{\partial u}{\partial x} + \dfrac{\partial v}{\partial y}\right) \\ \mu\dfrac{k\gamma}{Pr}\dfrac{\partial e_i}{\partial y} + \psi_2 \end{bmatrix}$$

where $\psi_1$ and $\psi_2$ are composed of the viscous dissipation terms in the energy equation and are given by

$$\psi_1 = 2\mu u\frac{\partial u}{\partial x} - \frac{2}{3}\mu u\left(\frac{\partial u}{\partial x} + \frac{\partial v}{\partial y}\right) + \mu v\left(\frac{\partial u}{\partial y} + \frac{\partial v}{\partial x}\right)$$

$$\psi_2 = 2\mu v\frac{\partial v}{\partial x} - \frac{2}{3}\mu v\left(\frac{\partial u}{\partial x} + \frac{\partial v}{\partial y}\right) + \mu u\left(\frac{\partial v}{\partial x} + \frac{\partial u}{\partial y}\right)$$

The equation of state for a perfect gas closes the above system of equations and can be written as follows:

$$p = (\gamma - 1)\rho e_i$$

with

$$e_i = \frac{e}{\rho} - \tfrac{1}{2}(u^2 + v^2)$$

## Acknowledgments

This investigation was carried out under the sponsorship of the National Aeronautics and Space Administration, through Grant NSG 3266, with Dr. P. M. Sockol as the Technical Monitor. The comments by the reviewers were helpful, and are included in this paper.

## References

[1]Denton, J. D., "A Time-Marching Method for Two- and Three-Dimensional Blade-to-Blade Flow," Aeronautical Research Council R&M 3775, 1975.

[2]Steger, J. L., Pulliam, T. H., and Chima, R. V., "An Implicit Finite-Difference Code for Inviscid and Viscous Cascade Flows," AIAA Paper 80-1427, 1980.

[3]Shamroth, S., Gibeling, H. J., and McDonald, H., "A Navier-Stokes Solution for Laminar and Turbulent Flow Through a Cascade of Airfoils," AIAA Paper 80-1426, 1980.

[4]Lakshminarayana, B. and Govindan, T. R., "Analysis of Turbulent Boundary Layer on Cascade and Rotor Blades of Turbomachinery," *AIAA Journal,* Vol. 19, Oct. 1981, pp. 1333-1341.

[5]Govindan, T. R., "A Space-Marching Method for the Navier-Stokes Equations for Internal Flows," Ph.D. Thesis, Department of Aerospace Engineering, The Pennsylvania State University, University Park, PA, 1983.

[6]Rakich, J. V., "Iterative PNS Method for Attached Flows with Upstream Influence," AIAA Paper 83-1955, 1983.

[7]Vigneron, Y. C., Rakich, J. V., and Tannehill, J. C., "Calculation of Supersonic Viscous Flow Over Delta Wings with Sharp Subsonic Leading Edges," NASA TM-78500, 1978.

[8]Beam, R. M. and Warming, R. F., "An Implicit Factored Scheme for the Compressible Navier-Stokes Equations," *AIAA Journal*, Vol. 16, April, 1978, pp. 393-401.

[9]Pouagare, M., "Numerical and Experimental Investigation of the Compressor Rotor Flow Field," Ph.D. Thesis, Department of Aerospace Engineering, The Pennsylvania State University, University Park, PA, 1984.

[10]Degani, D. and Steger, J. L., "Comparison Between Navier-Stokes and Thin-Layer Computations for Separated Supersonic Flow," *AIAA Journal*, Vol. 21, Nov. 1983.

[11]Anderson, O. L. et al., "Solution of Viscous Internal Flows on Curvilinear Grids Generated by the Schwarz-Christoffel Transformation," *Numerical Grid Generation*, Elsevier Science Publishing, 1982.

[12]Blottner, F. G., "Significance of the Thin-Layer Navier-Stokes Approximation," *Numerical and Physical Aspects of Aerodynamic Flows*, edited by T. Cebeci, Springer-Verlag, 1985.

[13]Schlichting, H., *Boundary-Layer Theory,* 7th Ed., McGraw-Hill Book Co., New York, 1979.

[14]Kreskovsky, J. P., Briley, W. R., and McDonald, H., "Turbofan Forced Mixer-Nozzle Internal Flow Field," NASA CR-3494, 1982.

[15]Herrig, L. J., Emery, J. C., and Erwin, J. R., "Systematic Two-Dimensional Cascade Tests of NACA 65-Series Compressor Blades at Low Speeds," NACA TN 3916, 1957.

[16]Speidel, L., "Berechrung der Stromungverluste von Ungestaffelten Ebenen Schaufelgittern," *Ing. Arch.,* Vol. 22, 295, 1954.

[17]Peterson, C. R., "Boundary Layer on an Airfoil in a Cascade," Gas Turbine Laboratory, Massachusetts Institute of Technology, Cambridge, MA, Rept. 49, Dec. 1958.

[18]Rothmayer, A. P. and Davis, R. T., "The High Reynolds Number Finite Flat-Plate Cascade," *AIAA Journal*, Vol. 21, May, 1985, pp. 758-759.